## SPI CALIBRATIONS

**4 STEPS** :

- **CAMERA CALIBRATION** :
After camera integration (Sept 2000)

- **SPI CALIBRATION AT CNES**
After SPI integration (Dec 2000)

- **SPI AT THERMAL TEST**
SPI in representative thermal conditions (March - April 2001)

- **SPI CALIBRATION AT BRUYERES LE CHATEL**
Latest calibration before SPI delivery at ESA (April - May 2001)

## SPI FM CALIBRATIONS

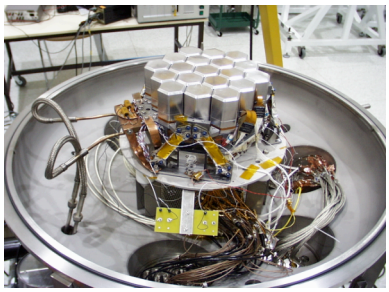

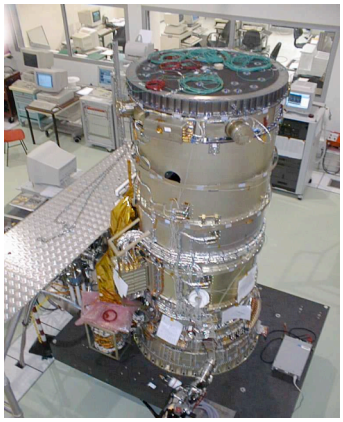

CALIBRATION SYSTEM :
GUN (Sources collimator)

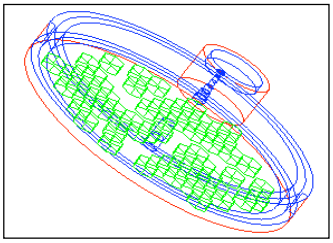

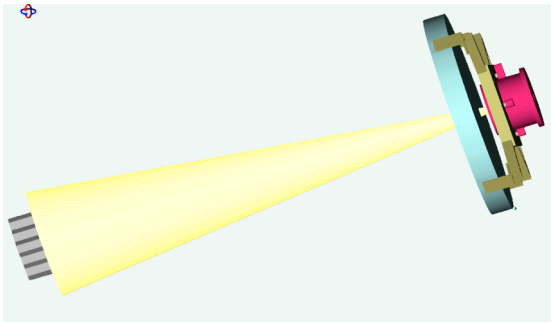

The following sources had been used :
$^{137}Cs$ / $^{60}Co$ / $^{241}Am$ / $^{24}Na$ / $^{85}Sr$ / $^{54}Mn$ / $^{88}Y$ / $^{109}$ Cd / $^{228}Th$ / $^{57}Co$

**Single event spectra simulation and measurement for the central detector. Radioactive source : $^{85}Sr$**

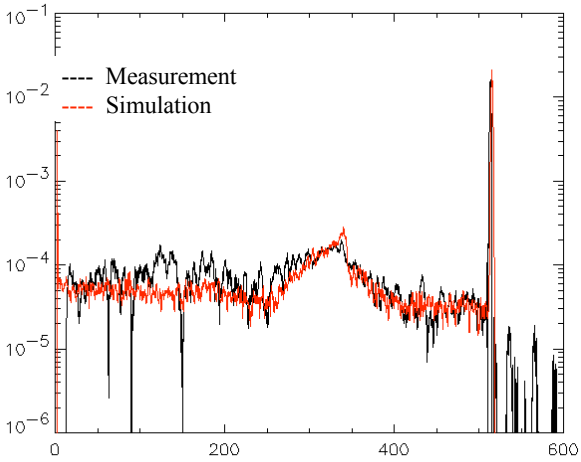

**SPI CALIBRATION AT BRUYERES LE CHATEL**
(May 2001)

# CALIBRATION SCHEME

**SPI without coded mask** : Test efficiency and homogeneity

- Short distance sources (low intensity, 8 m).

11 different radioactive sources . Energy range : [60,1836] keV.

- 4 MeV-van de Graaf accelerator, calibration up to 8062 keV.

**SPI with coded mask** : Test of imaging

- Long distance sources (high intensity,125 m),

Energy range : [60,2753] keV.

## IMAGING PERFORMANCES

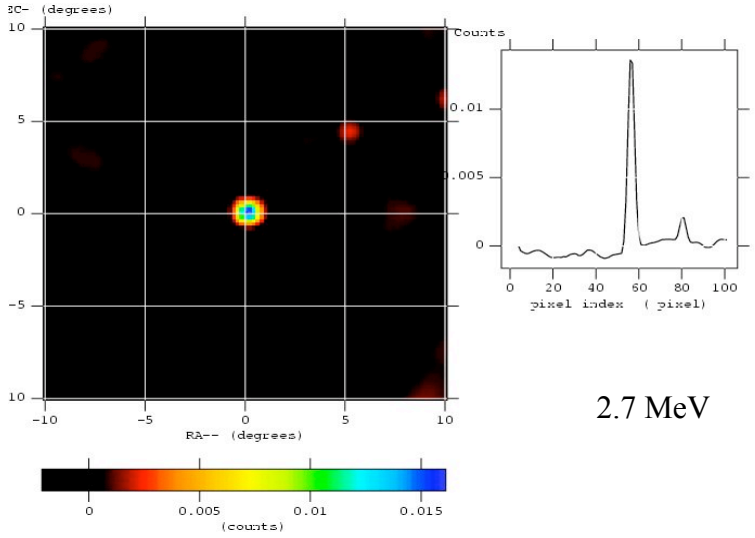


2.7 MeV

# Response matrix generation by Monte-Carlo simulation

# Instrument Response: Overview

- A detailed mass model was created “by hand” based on technical drawings.
- Several “compression” schemes were devised to make the MC problem manageable in terms of CPU and storage.
- Simulations of the BLC calibration were performed at GSFC using the mass model and “MGEANT” MC SW.
- Comparison of these simulations with data led to improvements in the MC software and the mass model.

# Instrument Model

These cutaway views give an idea of the level of detail in the SPI instrument model, which has been integrated with the Southampton “TIMM”.

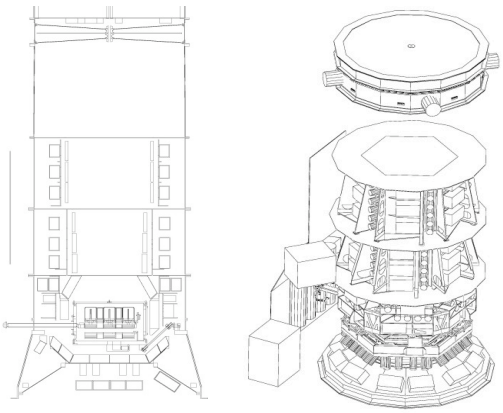

SPI cut-away views

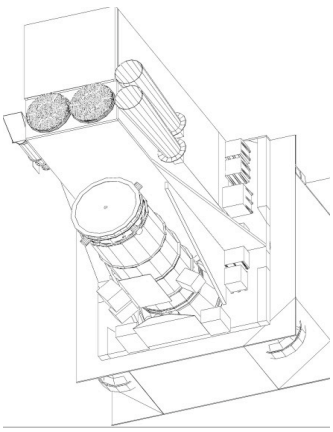

TIMM-3

# Instrument Response Corrections

**Mask honey-comb support transmission correction curve. Points are the measurements for 4 offset angles, and the curves are from MC simulations.**

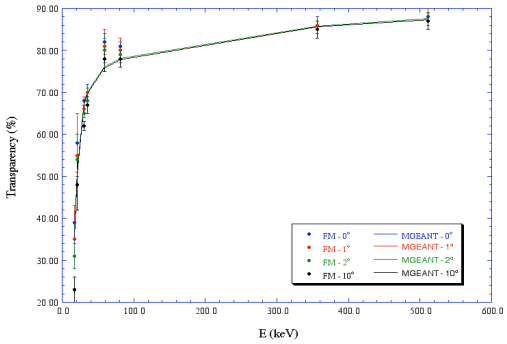


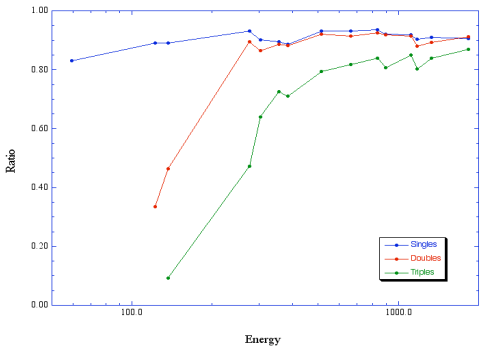


Photo-peak effective area correction factors for single, double & triple events. Extrapolation to Lowest and highest energies.

# IRF Compression

- The computational problem scales as ~$N_{sky}$ x $N_{det}$ x $N_{ch}$, per mono-energetic input energy with statistics at each vertex, which becomes unmanageable
- Savings was achieved first, by tracking detailed MC events for vertices within single a “pie-wedge” subset of the detector array
- This is then convolved with a full (i.e. all directions) database of absorption path-lengths derived from the ray-tracing events

# IRF Compression

- This leads to 2 large, databases of
  - spectra per detector-array vertex per direction (DMATRIX)
  - absorption path lengths per direction (over sampling instrument resolution by ~5X (LMATRIX)
- From these, the basic response data set, or IRF is created
  - 5 dimensional object, $N_E$ x $N_\theta$ x $N_\phi$ x $N_{det}$ x $N_{spc\text{-}cmp}$
  - this comprises the basic end-user response database which is used directly in image reconstruction
  - and from which XSPEC "ARFs" are extracted

# Response Decomposition

The response is approximated as a convolution of ray-tracing and detailed photon-propagation terms:

$$R(d,\theta,\phi,E,ch) = \sum L_i(d,\theta,\phi,E) \cdot D_i(d,\theta,\varphi,E,ch)$$

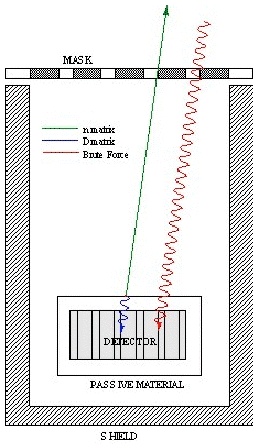


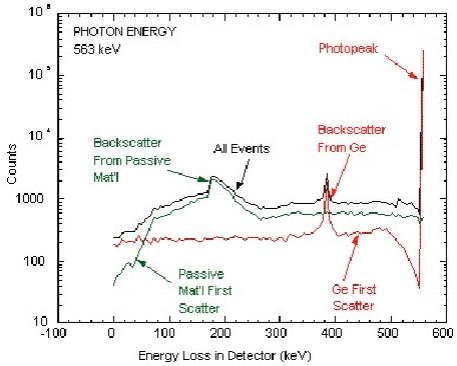


Further computational and storage economy are achieved by recognizing that the response continuum can be reconstructed as a linear combination of components.

# IRF Calibration

On-axis, total efficiency. Blue is uncorrected IRFs. Data points are $^{133}$Ba and $^{241}$Am measurements from CEA. Red curve is the re-calibrated IRF.

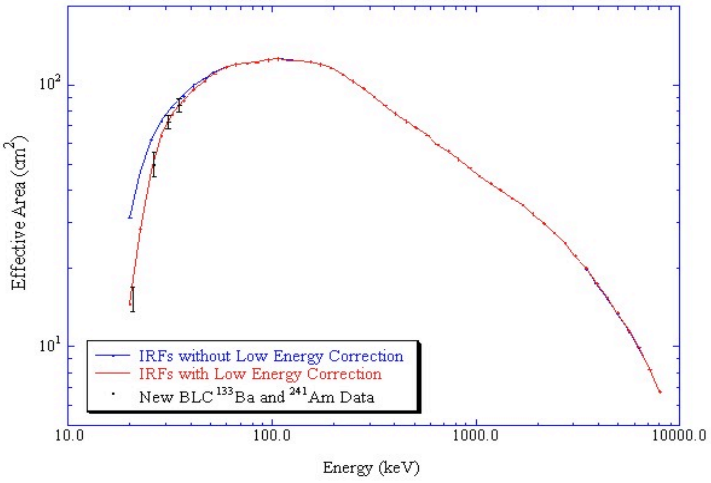


# SPECTRAL DECONVOLUTION

- Source counts are extracted using the ARF corresponding to the full energy peak
- All the SCW's are fitted simultaneously
- A mean response matrix with the counts redistribution is computed for the source position and the pointing history.
- The spectrum is extracted by model fitting through this matrix

# SPI Crab Nebula observations

## THE CRAB NEBULA 20-50 keV 567 ks

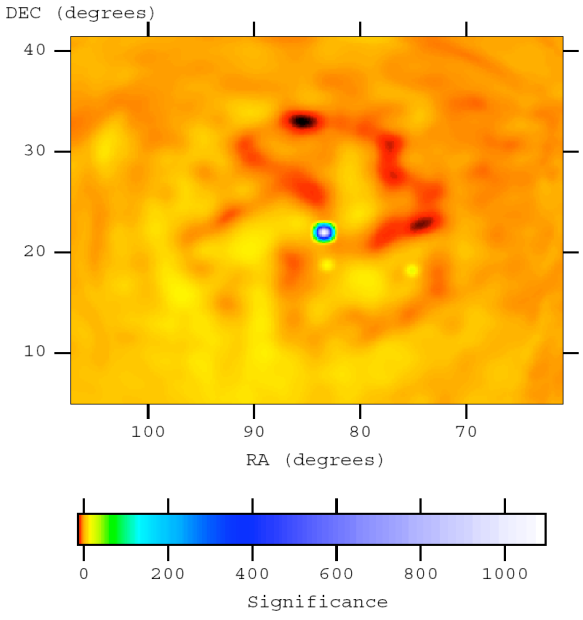

Crab Nebula

Stability in the FOV
Rev 300

10° circle around the axis

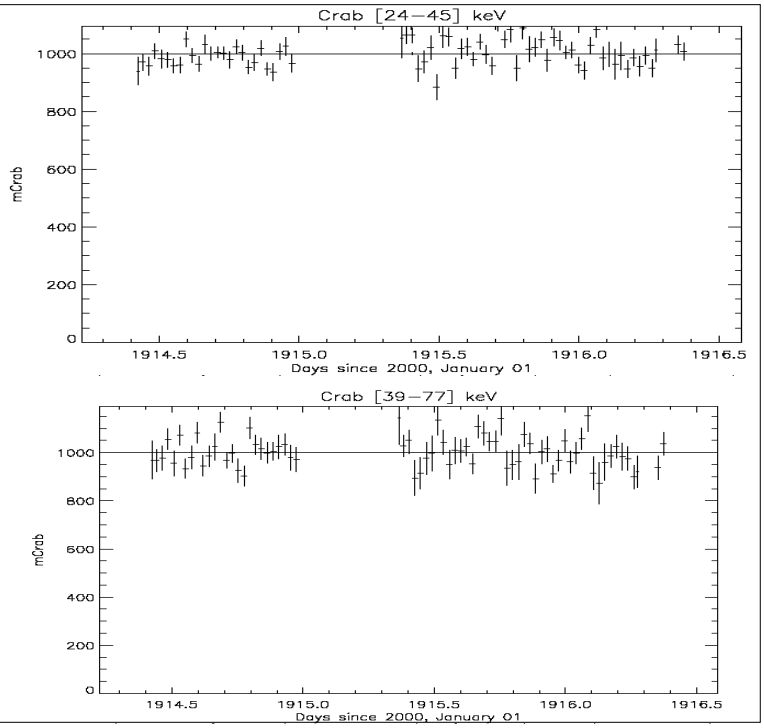


## Crab Nebula - Calibration stability – revolutions 300 and 45

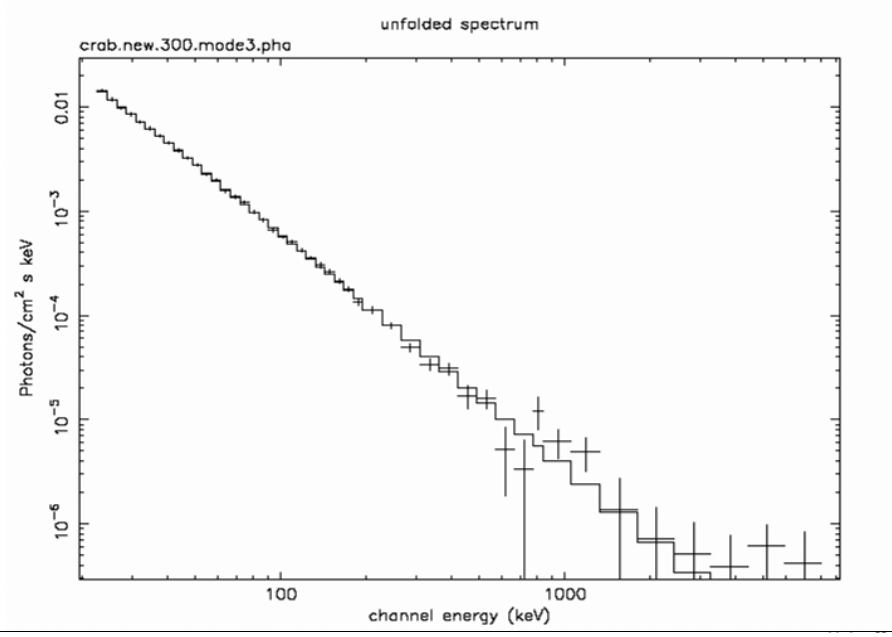

# Crab spectral fits

- Energy range 22 keV – 1 MeV
- Use of single events
- No systematics included
- Source and background assumed constant per revolution
- Use of standard response matrices
- Since SVR: improvement of matrices interpolation.

| Rev # | Index 1 | Ebreak (keV) | Index 2 | Norme @ 100 keV (ph cm-2 s-1) | Red $\chi$ 2 (35 dof) | Ftest Relat. To powerla w |
|---|---|---|---|---|---|---|
| 44 | 2.06 +/- 1.10 $^{-2}$ | 66 +/- 3 | 2.22 +/- 2.10 $^{-2}$ | 6.27 E-04 | 1.98 | |
| 45 | 2.05 +/- 1.10 $^{-2}$ | 70 +/- 2 | 2.25 +/- 1.10 $^{-2}$ | 6.4 E-04 | 2.15 | |
| 102 | 2.07 +/- 1.10 $^{-2}$ | 66 +/- 3 | 2.22 +/- 2.10 $^{-2}$ | 6.19 E-04 | 1.26 | |
| | | | | | | |
| 170 | 2.06 +/- 1.10 $^{-2}$ | 66 +/- 2 | 2.22 +/- 1.10 $^{-2}$ | 6.33 E-04 | 1.93 | |
| | | | | | | |
| 239 | 2.07 +/- 1.10 $^{-2}$ | 63+/- 2 | 2.23 +/- 1 10 $^{-2}$ | 6.25 E-04 | 1.82 | 4.3 E-08 |
| 300 | 2.07 +/- 1.10 $^{-2}$ | 60 +/- 2 | 2.23 +/- 1 10 $^{-2}$ | 6.12 E-04 | 1.87 | 3.2 E-06 |
| 365 | 2.11 +/- 1.10 $^{-2}$ | 152+/- 13 | 2.70 +/- .13 | 6.23 E-04 | 1.83 | 3.1 E-05 |
| 365* | 2.08 +/- 1.10 $^{-2}$ | 71 +/- 7 | 2.27+/- 3 10 $^{-2}$ | 6.05 E-04 | 2.32 | 2. E-03 |
| 422 | 2.09 +/- 1.10 $^{-2}$ | 68 +/- 2 | 2.25 +/- 1.10 $^{-2}$ | 6.16 E-04 | 1.92 | 2. 9 E-06 |
| 483 | 2.13 +/- 2.10 $^{-2}$ | 88 +/- 18 | 2.29 +/- 5.10 $^{-2}$ | 6.00 E-04 | 2.10 | 0.01 |
| 541(tr) | 2.06 +/- 1.10 $^{-2}$ | 65 +/- 3 | 2.23 +/- 1 10 $^{-2}$ | 6.06 E-04 | 1.78 | |
| Sum | 2.09 +/- 2.10 $^{-2}$ | 69 +/- 2 | 2.25 +/- 2.10 $^{-2}$ | 5.98 E-04 | 5.42 | 7.7 E-08 |

# Rev. 239+300+365+422+483 - 530ks

| Rev # | Index 1 | Ebreak (keV) | Index 2 | Norme @ 100 keV (ph cm-2 s-1) | Red $\chi$ 2 | Ftest Relat. To powerlaw |
|---|---|---|---|---|---|---|
| Sum | 2.14 +/-2. 10 $^{-2}$ | | | 6.01 E-04 | 13.06 | |
| Sum | 2.11 +/- 1.10 $^{-2}$ | 90.0 | 2.30 +/- 1.10 $^{-2}$ | 6.1 E-04 | 5.38 | 1.2 E-08 |
| Sum | 2.09 +/- 2.10 $^{-2}$ | 69 +/- 2 | 2.25 +/- 2.10 $^{-2}$ | 5.98 E-04 | 5.42 | 7.7 E-08 |

The power-law is rejected

The broken power law better represents the data (physics behind?)

The broken power law break is not precisely constrained: slopes/break dependency

## SUM Rev 239 -- 483

**Model PL**

Index 2.14 +/- 2.5E-03

$\chi$2= 483.4 using 39 bins.
Reduced $\chi$2 = 13.06 for 37 DoF
Null hypothesis probability = 0.0

**Model broken PL**

Index1 2.08814 +/- 5. E-03
E Break 68.8701 +/- 2.32937 keV
Index2 2.25263 +/- 0.1
$\chi$2= 189.7 using 39 bins.
Reduced $\chi$2 = 5.42 for 35 DoF
Null hypothesis probability = 3.785E-23

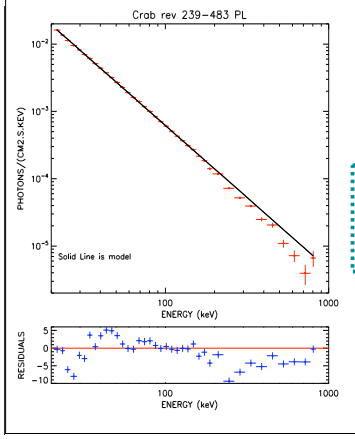


**F- test**

F statistic value = 27.1
probability = 7.8 E-08